communications chemistry

A Nature Portfolio journal

Article

https://doi.org/10.1038/s42004-025-01823-5

Site- and conformer-specific reaction dynamics of glycine with the hydroxyl radical

Balázs Gruber & Gábor Czakó

Understanding the state-to-state atomic-level dynamics of a chemical reaction is a central topic in modern chemistry. Moving beyond the traditional mode-specific reaction dynamics studies, here we investigate the concept of site and conformer specificity by studying the reaction of the glycine molecule (H_2NCH_2COOH) with the hydroxyl (OH) radical using first-principles theory. Conformer-specific quasi-classical trajectory computations on a 30-dimensional potential energy surface reveal three distinct H-abstraction pathways targeting the different functional groups. CH_2- and NH_2-H-abstraction proceed through direct, single-step mechanisms, whereas a two-step mechanism emerges for COOH-H-abstraction, where initial dehydrogenation frequently leads to fragmentation into CO_2 and CH_2NH_2. COOH-H-abstraction is favored at low energies, while NH_2- and CH_2-H-abstraction are promoted at higher energies. The formation of the unstable $H_2NCH_2COO•$ intermediate becomes increasingly restricted at higher collision energies due to limited interaction time. In specific reactant conformers, the simulations reveal an indirect biradical mechanism and an alternative stabilization pathway via intramolecular H transfer. Product-conformer distributions exhibit a three-step pattern of carboxyl group rearrangement—H-orientation switch, 180° rotation around the C–C axis, and their combination—during NH_2- and CH_2-H-abstraction. Structure-specific product formation arises clearly only in CH_2-H-abstraction, driven by the closed COOH conformation, whereas NH_2-H-abstraction leads to conformational diversity in the products.

One of the main goals of chemistry is to understand processes in nature at the deepest atomic and molecular level. Moving beyond the traditional kinetics studies, which follow concentration of chemical species in time, modern reaction dynamics investigations can reveal the motion of atoms in chemical processes using either experimental or theoretical methods. Crossed-beam experiments[1–3] are capable to detect the outcome of single collision events, while classical and/or quantum simulations[4–15] can follow the atomic-level reaction pathways from reactants to products. The accurate simulations began with the $H + H_2$ reaction[4] in the 1970s and arrived to the reactions of small organic molecules such as CH_4[5–8], CH_3Cl[9], CH_3I[3,10], C_2H_6[11,12], CH_3OH[8,13], CH_3CH_2Cl[14,15], etc. with simple radicals like H[6,8], F[7,8,13], Cl[5,8,11], OH[8,12] and/or ions like F^-[9,10,14], Cl^-[3], OH^-[15] in the past 10–20 years. In the case of polyatomic reactants mode-specific dynamics investigations are also possible, where the influence of the initial excitation of different vibrational modes on the dynamics is studied[5,7–9,11,13]. Moreover, even state-to-state dynamics can be described, thereby tracking the mode-specific energy flow from reactants to products[2,5,16,17].

In the present study we increase the complexity of the reactant by studying the dynamics of the reaction of glycine (H_2NCH_2COOH) with the OH radical. The glycine molecule has eight conformers with different structures and energies[18,19], which introduce a novel aspect to the dynamics as the various conformers may have different reactivities. Conformer specificity is not an unknown concept[20–23], though it has not been as thoroughly explored as vibrational mode-specificity. Therefore, we aim to set a new level of insight about conformer-specific reactivity by investigating the reaction of different glycine conformers with OH showing how the initial selection affects the conformer distribution of the products. Furthermore, the title reaction has multiple competitive reaction pathways describing hydrogen abstraction from the various sites (functional groups) of glycine, which adds to the complexity of the system. So far only the conformers of the reactants[18,19,24–26], products[27–33] and transition states and post-reaction complexes[28,34,35] of the OH + glycine reaction were characterized in the literature, dynamics simulations have not been reported. Of course, such simulations are extremely challenging due to the above-mentioned

MTA-SZTE Lendület "Momentum" Computational Reaction Dynamics Research Group, Interdisciplinary Excellence Centre and Department of Physical Chemistry and Materials Science, Institute of Chemistry, University of Szeged, Szeged, Hungary. e-mail: gczako@chem.u-szeged.hu

complexity of the title reaction. One has to sample a large configuration space in 30 dimensions, and deal with complicated electronic structure computations of an open-shell system to obtain a potential energy surface (PES) which governs the motion of the nuclei in the chemical reaction. In the present study we carry out such simulations using the gold-standard of electronic structure methods[36] and an analytical representation of the PES allowing efficient dynamics simulations revealing site and conformer specificity in the atomic-level mechanisms of the title reaction. Furthermore, we show how these simulations can uncover new, unexpected chemistry in a reaction.

Results and discussion

During the mapping of the PES for the OH + glycine H-abstraction reaction, we considered three distinct product channels[35]. In each case, the hydroxyl radical removes a H atom from one of the three functional groups of glycine—the amino (NH_2), methylene (CH_2), or carboxyl (COOH) group—resulting in the formation of H_2O and a dehydrogenated glycine molecule, with the abstraction site dictating the specific product formed. Interestingly, the present quasi-classical trajectory (QCT) simulations on a newly-developed high-level ab initio full-dimensional PES reveal that the H-abstraction reaction at the carboxyl group can follow a more complex mechanism than previously anticipated. Instead of stopping at the initial step, the dehydrogenated glycine molecule formed via COOH abstraction can undergo further decomposition, breaking apart into CO_2 and CH_2NH_2. Figure 1 presents the structures and relative classical energies of the stationary points along all identified OH + glycine H-abstraction reaction channels, comparing the benchmark potential energy values from our previous study[35] (shown in black) with the analytical PES-derived energies (shown in green). The energies of the previously unconsidered products ($H_2O + CO_2 + CH_2NH_2$) are also determined at the same theoretical level as the benchmark mapping. The multi-reference characters of the stationary points (Supplementary Fig. 1) and the root-mean-squares fitting errors are shown in Supplementary Tables 1 and 2, respectively. The small energy differences observed between most of the benchmark and PES energies further validate the accuracy of the developed PES. The somewhat larger deviation in the case of the three-fragment products is due to the fact that this channel was automatically developed without manually adding any geometry to this region. The PES also well describes the various conformers of the stationary points as shown in Supplementary Table 3 in the case of the glycine molecule. Among the three H-abstraction pathways, only the reaction at the carboxyl group exhibits a very low barrier. However, when zero-point energy (ZPE) is taken into account, the carboxyl-mediated pathway also becomes kinetically barrierless. It can be concluded that all three reactions are exothermic. When considering only the dehydrogenation step, H abstraction from the CH_2 group releases the most energy, followed by the NH_2 and COOH pathways. However, taking into account the subsequent decomposition of the glycine molecule dehydrogenated at the carboxyl group, this process becomes thermodynamically more favorable than H abstraction at the NH_2 group.

Figure 2 provides insight into how the conformer-specific integral cross section (ICS) varies with increasing collision energy (E_{coll}) for each reaction channel, distinguishing eight cases based on trajectories initiated from distinct glycine conformers. The statistical uncertainty of the ICSs can be assessed based on Supplementary Table 4. When the hydroxyl radical targets the carboxyl group of glycine, the reaction rarely stops at the initial dehydrogenation step. More often, it continues with the decomposition of the dehydrogenated glycine molecule, ultimately yielding H_2O, CO_2, and CH_2NH_2 as products. Furthermore, at low collision energies, particularly at E_{coll} = 1 kcal/mol, the three-fragment product channel exhibits markedly higher reactivity compared to H abstraction at the amino and methylene groups. With increasing collision energy, the reactivity of H abstraction at the carboxyl group gradually declines, eventually reaching a plateau where the ICS stabilizes. Meanwhile, the H-abstraction reactions at the amino and methylene groups become progressively more prominent. The reaction at the CH_2 group emerges as the most dominant, driven by its thermodynamic favorability, as it releases the highest amount of energy. It can be concluded that the overall profile of the cross section curves remains consistent across all glycine conformers, regardless of the initial structure from which the trajectories are initiated, with only minor differences in absolute reactivity.

Figure 3 displays the opacity functions, illustrating the reaction probability as a function of the impact parameter for the reaction of OH with the lowest-energy glycine conformer (Ip), with distinct curves representing H abstraction from the amino, methylene, and carboxyl groups. Opacity functions for all the initial glycine conformers are shown in Supplementary Fig. 2. (Interested readers may also consult with Supplementary Fig. 3 for conformer-specific scattering angle distributions.) The reaction probability curves for H abstraction at the NH_2 and CH_2 groups exhibit similar profiles, whereas the reactivity of the COOH group follows a distinct pattern. For NH_2- and CH_2-H-abstraction, the maximum impact parameter (b_{max})—the critical perpendicular distance between the velocity vectors of the reactants at which the reaction can still occur—remains constant regardless of the collision energy. In contrast, for H abstraction at the COOH group, b_{max} decreases with increasing collision energy, highlighting its strong collision energy dependence. The energy dependence may originate from the complex nature of the COOH pathway, where the initial H abstraction is inevitably followed by the fragmentation of the dehydrogenated glycine into CO_2 and CH_2NH_2. Unlike NH_2- and CH_2-abstraction, which terminate after H transfer, the $H_2NCH_2COO\bullet$ intermediate is inherently unstable and

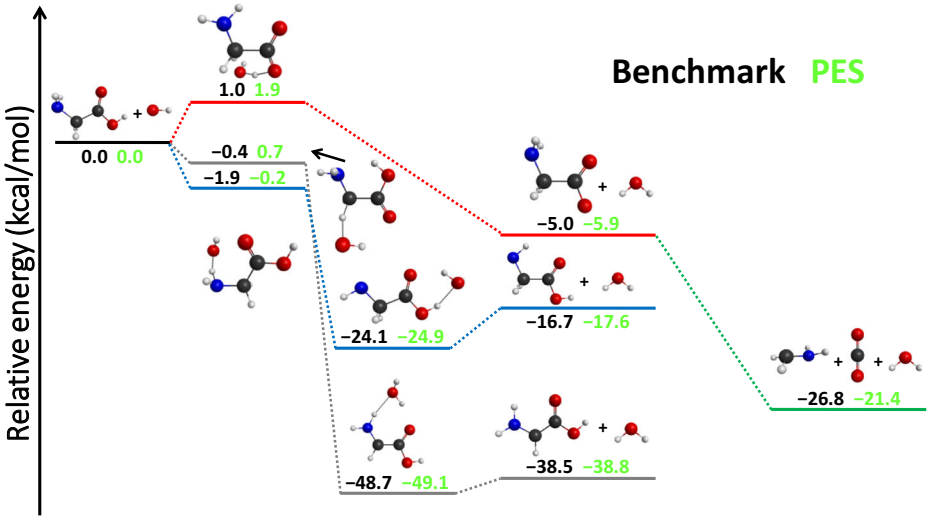

Fig. 1 | Schematic potential energy surface of the OH + glycine H-abstraction reaction. Reaction pathways showing the most accurate geometries of the lowest-energy conformers of the stationary points and displaying the previously-determined[35] benchmark classical relative energies in black and the values calculated using the present analytical PES in green.

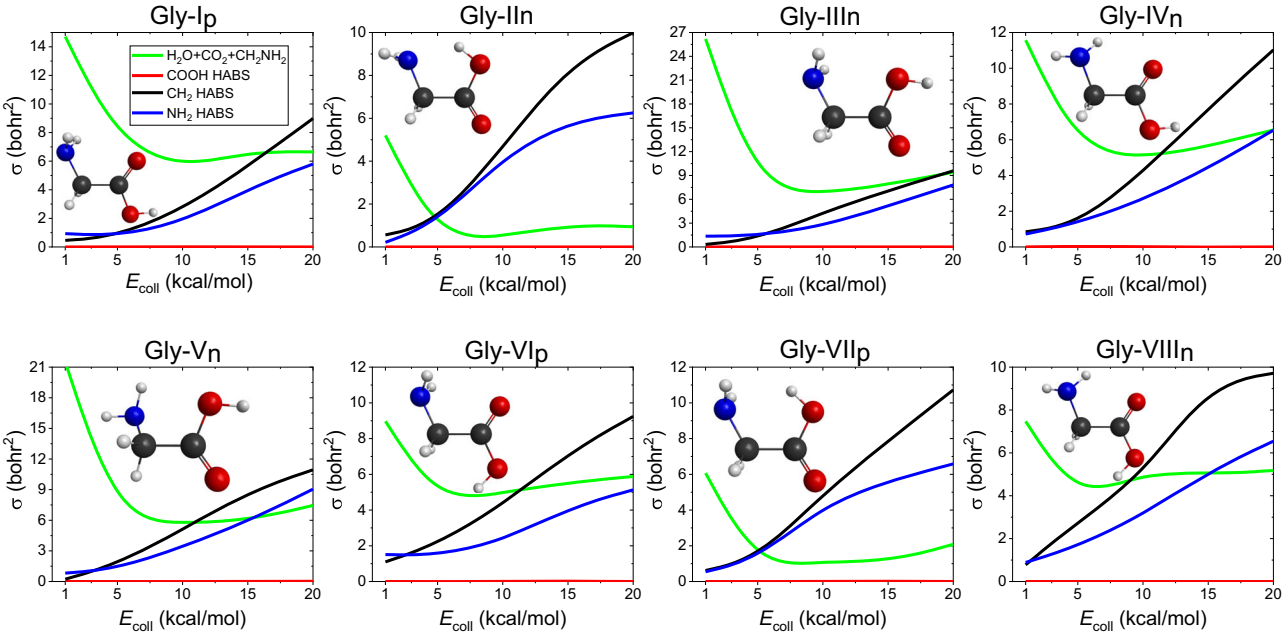

Fig. 2 | Site- and conformer-specific reactivity of the OH + glycine system. Integral cross sections as a function of collision energy for the various pathways of the OH + glycine H-abstraction reaction, with each panel specifying a different initial glycine conformer (see insets) denoted by roman numbers in increasing energy order indicating its planar (p) and non-planar (n) symmetry. Numerical values are given in Supplementary Data 2.

rapidly decomposes. At low collision energies, longer interaction times allow efficient energy redistribution within the system, facilitating reaction even at larger impact parameters, maintaining a high b_{max}. As collision energy increases, the interaction time shortens, limiting the redistribution of internal energy needed for this process, particularly at larger impact parameters. As a result, CO_2 production is increasingly restricted to smaller impact parameters, leading to a decrease in b_{max}. For NH_2- and CH_2-abstraction, the reaction follows a single H-abstraction step, where success depends solely on effective approach geometry. The trends observed in the ICSs further reflect these differences. At low collision energies, COOH abstraction dominates due to prolonged interaction. As energy increases, the ICS for the complex COOH abstraction decreases, while NH_2- and CH_2-H-abstraction become more prominent. At high collision energies, H abstraction at the NH_2- and CH_2-groups dominates, with the CH_2 pathway being significantly more favored due to its much higher thermodynamic driving force compared to NH_2-H-abstraction.

Figure 4 illustrates the initial attack angle (α) distributions of the reactants at collision energies of 10, 15, and 20 kcal/mol, providing insight into how the orientation of reactants influences reactivity and the angular preferences of reactive encounters. The left column presents the distribution for the OH radical, while the right column shows the corresponding distribution for the Ip conformer of the glycine molecule. Each row represents a different reaction pathway, distinguishing H abstraction from the NH_2, CH_2, and COOH groups, with the latter ultimately leading to the formation of H_2O, CO_2, and CH_2NH_2. For the OH radical, a cos(α) value of −1 signifies an approach where the O atom is directed toward the glycine molecule, whereas a cos(α) value of 1 corresponds to an approach from the H-side. The attack angle distributions remain largely isotropic across all three reaction pathways, indicating no strong preference for a specific orientation. At 10 kcal/mol, where NH_2-H-abstraction exhibits low reactivity, the peak observed around $\cos(\alpha) \approx -0.2$ is unlikely to reflect a mechanistic trend. In COOH-H-abstraction, a slight tendency for H-side approaches appears at the lowest collision energy, though statistical fluctuations may influence this observation. For the glycine molecule, a cos(α) value of −1 indicates an approach from the amino-side parallel to the C−C bond, while a value of 1 corresponds to an orientation where the carboxyl group faces the OH radical. When H abstraction occurs at the NH_2 group, higher collision energies (15 and 20 kcal/mol) disfavor amino-side approaches parallel to the C−C bond. The lone pair on the amino-N may facilitate H-bonding with the H of the OH radical, potentially stabilizing approach geometries that lead to reactivity. For H abstraction at the CH_2 group, glycine preferentially approaches with the H_2NCH_2 part directed toward the OH radical across all collision energies, rather than from the carboxyl-side. The spatial arrangement of the CH_2-H atoms in this configuration allows for more efficient access by the OH radical, increasing the probability of successful abstraction. Additionally, H-bonding between the NH_2-N and the H of the OH may further contribute to the stability of this orientation, increasing the likelihood of reactivity. For COOH-H-abstraction, glycine predominantly approaches with the carboxyl group facing the OH radical. The O atoms of the carboxyl group can engage in H-bonding with the H of the OH radical, which may enhance attraction and promote an orientation favorable for abstraction.

Surprisingly, the initial attack angle distributions of glycine in COOH-H-abstraction reactions do not always follow the expected pattern. Instead of predominantly approaching the OH radical from the carboxyl side, certain conformers—specifically IIn and VIIp—exhibit a greater tendency to interact from the amino side (see Supplementary Fig. 4). Reaction dynamics simulations reveal that, despite this unexpected orientation, H abstraction still occurs at the carboxyl group. However, the process follows an indirect route: a hydrogen first migrates from the carboxyl group to the amino group, forming a biradical intermediate (H_3N–CH_2–COO), from which the OH radical subsequently abstracts a hydrogen. Figure 5 presents selected trajectory snapshots capturing the formation of the biradical intermediate and the final abstraction step in reactions involving the IIn and VIIp glycine conformers. An important question arises: what drives the formation of the biradical intermediate? The molecular structure of the IIn and VIIp glycine conformers (see Fig. 2) provides the key, as both adopt a geometry where the carboxyl-H is positioned near the amino-N, facilitating internal hydrogen transfer and creating favorable conditions for the emergence of the biradical pathway. Animations reveal that (22, 33, 14, 10, 7)/(26, 35, 18, 12, 9) % of the OH + Gly(IIn/VIIp) trajectories forming $H_2O + CO_2 + CH_2NH_2$ products proceed via a biradical structure at collision energies of (1, 5, 10, 15, 20) kcal/mol. However, as Supplementary Fig. 5 shows the fitted PES substantially underestimates the ab initio energies

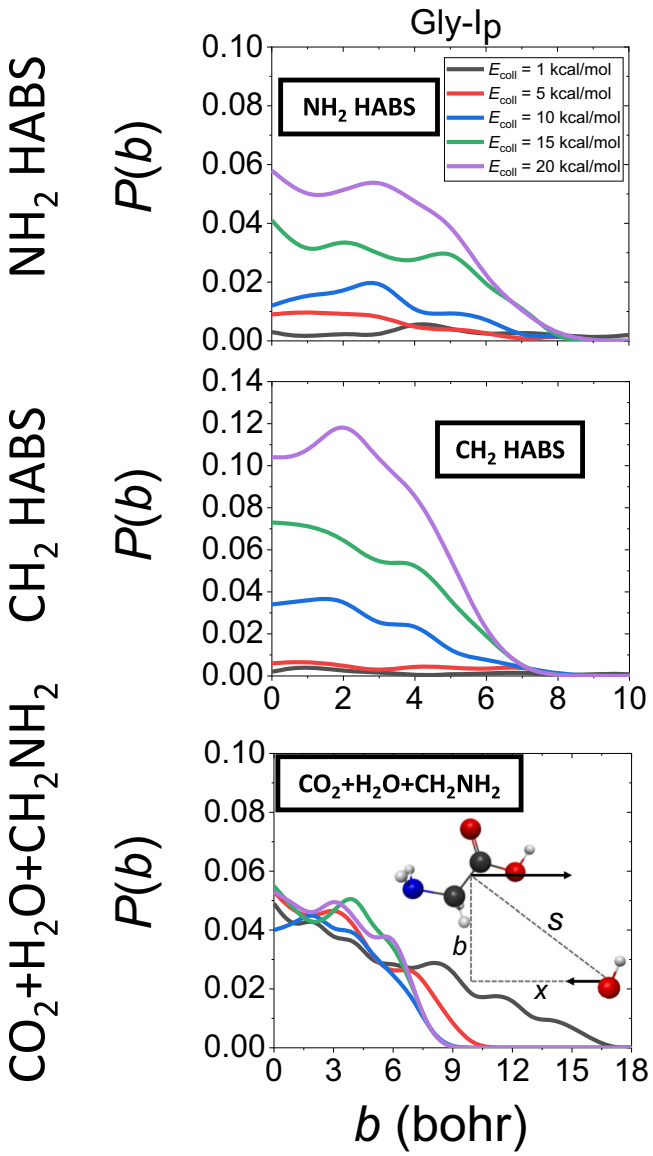

Fig. 3 | Site-specific opacity functions for the OH + glycine(Ip) system. Reaction probabilities as a function of the impact parameter (b) for the OH + Ip glycine conformer H-abstraction reaction at collision energies of 1, 5, 10, 15, and 20 kcal/mol. Numerical values are given in Supplementary Data 2.

at the intramolecular hydrogen transfer region, indicating that the significance of the biradical pathways may be overestimated and future work is warranted to confirm this novel mechanism.

We have also investigated the possible indirect pathways of the $H_2NCHCOOH$ and $HNCH_2COOH$ product formations. On one hand, trajectory animations show that the former products are always obtained through direct H abstraction from the CH_2 group. We have not found any H transfer pathways from CH_2 to the dehydrogenated amino or carboxyl group presumably due to steric reasons. On the other hand, animations reveal that in the case of the IIIn and Vn glycine conformers the $HNCH_2COOH$ products can be obtained via an indirect, low-probability pathway, where OH abstracts a hydrogen atom from the COOH group while an intramolecular H transfer occurs from NH_2 to COO as shown in Fig. 6. H transfer from NH_2 (or COOH, which would lead to CO_2 formation) to the dehydrogenated CH_2 group is not found, as expected, because of both thermodynamic and steric reasons.

Figure 7 illustrates the probability of forming different product conformers during NH_2- and CH_2-H-abstraction reactions, depending on the initial reactant conformers. The probabilities of product conformer formation during both NH_2-H-abstraction and CH_2-H-abstraction from different glycine conformers reveal a three-step pattern, where reactant conformers pair up based on their nearly identical likelihood of producing the same product conformer. Each pair shares the same carboxyl group spatial arrangement, emphasizing its key role in governing reaction dynamics. The observed pattern also reflects the sequential structural changes the carboxyl group undergoes during H abstraction. The first and most probable step, progressing from top to bottom, involves a rearrangement of the carboxyl-H atom, followed by a 180° rotation of the entire carboxyl group around the C–C axis, while the final step captures the simultaneous occurrence of both transformations. The magnitude of each step carries significant information, offering insights into the strength of intramolecular stabilizing forces. The observed differences indicate which structural arrangements are more favorable and which provide less stabilization for either the initial or final conformation. The magnitude of the first step, associated with the probability of rearranging the carboxyl-H spatial orientation, follows a consistent pattern in both NH_2- and CH_2-H-abstraction reactions. The observed trend indicates that the closed conformation of the carboxyl group, where the carboxyl-H points toward the carbonyl-O, exhibits greater stability compared to the open conformation. Product distribution data provide clear support for this conclusion, as both NH_2- and CH_2-H-abstraction reactions show that starting from a reactant conformer with a closed carboxyl group results in a relatively low probability of switching to an open conformation in the product. Conversely, reactant conformers with an open carboxyl group exhibit a relatively high probability of forming a product conformer in the closed conformation. The magnitude of the second step, which corresponds to product formation from reactants with the third-highest formation probability, reveals that a 180° rotation of the entire carboxyl group around the C–C axis is exceptionally rare in CH_2-H-abstraction reactions, occurring in no more than 5-6% of cases. In contrast, NH_2-H-abstraction follows the same trend for nearly all products, except for the formation of amino-product IV and V. The explanation lies in the nature of H abstraction and its impact on stabilizing H-bonds within the glycine molecule. During CH_2-H-abstraction, hydrogen removal does not disrupt these stabilizing interactions, allowing them to maintain the integrity of the product structure. However, NH_2-H-abstraction directly affects one of the H-bond centers. The departure of a hydrogen atom results in increased mobility for the remaining hydrogen, potentially introducing a repulsive interaction between the amino-N and either the carbonyl- or hydroxy-O. Analysis of the molecular interactions reveals that a stronger destabilizing effect arises when the hydroxyl-O is positioned opposite the amino-N, compared to when the carbonyl-O is in the same position. The increased repulsion in the former arrangement forces the amino-N to deviate significantly from the C-C-O plane, contributing to reduced structural stability. While the previous analysis focused on identifying patterns in the distribution of product conformers for a given product, a complementary approach provides further insights into the factors influencing selectivity in NH_2- and CH_2-H-abstraction reactions. Examining the probabilities of forming each possible product conformer from a specific reactant conformer allows for the identification of structural features that govern selectivity. A fundamental observation is that high selectivity in H-abstraction reactions is only possible when hydrogen abstraction occurs at the CH_2 group. The Ip, IIIn, IVn, and Vn reactant conformers strongly indicate that the closed conformation of the carboxyl group serves as the driving force behind selectivity in CH_2-H-abstraction. In contrast, reactions starting from IIn, VIp, VIIp, and VIIIn reactant conformers, where the glycine molecule adopts an open carboxyl conformation, exhibit lower selectivity, as the formation probabilities of two different product conformers remain nearly equal, preventing the dominance of a single product structure. The lack of high selectivity in NH_2-H-abstraction can be attributed to the disruption of the hydrogen bond network that stabilizes the glycine molecule.

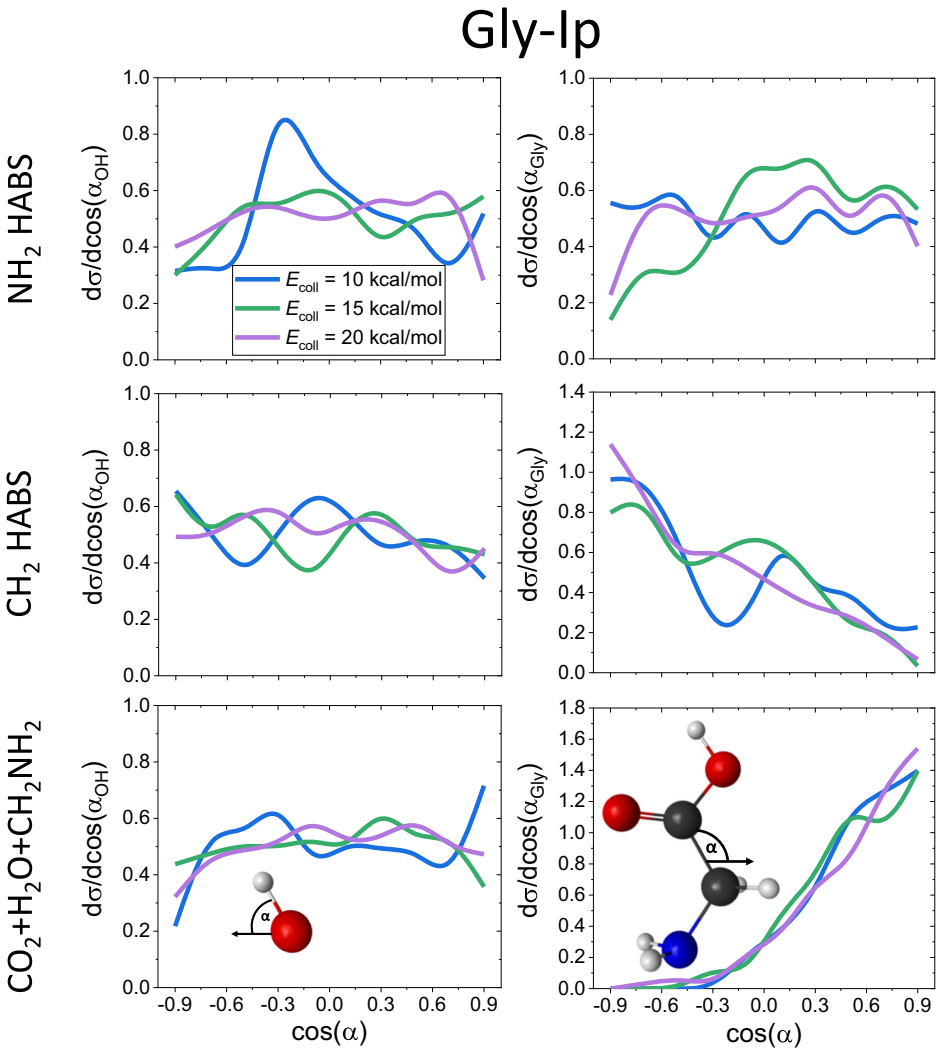

Fig. 4 | Orientation-dependent reactivity of the OH + glycine(Ip) system. Normalized initial attack angle distributions of the reactant OH (left-side) and Ip glycine conformer (right-side) for the OH + glycine H-abstraction reaction at collision energies of 10, 15, and 20 kcal/mol. Each row represents a different product channel. Numerical values are given in Supplementary Data 2.

H abstraction at the amino group increases the mobility of the remaining amino-H, facilitating interactions between the amino-N and either the hydroxyl-O or carbonyl-O, which introduce destabilizing effects and promote structural variations in the products.

Conclusions

A newly developed full-dimensional PES and QCT simulations are used to investigate the site- and conformer-specific dynamics of the OH + glycine H-abstraction reaction. The analysis focuses on three distinct pathways, targeting the amino (NH_2), methylene (CH_2), and carboxyl (COOH) groups. All three reaction channels are exothermic, with CH_2-H-abstraction releasing the highest amount of energy, followed by NH_2- and COOH-H-abstraction. Simulations reveal that COOH-H-abstraction rarely terminates at the initial dehydrogenation step, as the resulting glycine intermediate often fragments further, leading to CO_2 and CH_2NH_2 formation. Integral cross-section analysis shows a strong dependence on collision energy. At low energies, COOH-H-abstraction dominates. Increasing the collision energy reduces the likelihood of COOH-H-abstraction, while NH_2- and CH_2-H-abstraction pathways become progressively more significant. At higher energies, CH_2-H-abstraction prevails as the most favorable channel, primarily due to its thermodynamic advantage. The overall trends in ICS-s remain consistent across different initial glycine conformers, with only minor variations in absolute reactivity. Opacity functions provide insight into the relationship between reaction probability and impact parameter. The nearly constant maximum impact parameter (b_{max}) observed for NH_2- and CH_2-H-abstraction across all collision energies suggests that reaction efficiency is primarily governed by approach geometry. In contrast, COOH-H-abstraction displays a decreasing trend in b_{max} with increasing collision energy. Shorter interaction times at higher energies hinder the redistribution of internal energy necessary for CO_2 elimination, leading to a progressive shift in reaction toward smaller impact parameters. Attack angle distributions provide valuable insight into how molecular orientation influences reactivity. The analysis reveals that reaction outcomes depend primarily on the initial structure of glycine rather than the approach direction of the OH radical, with the extent of this effect varying across different reactant conformers. The initial conformer-specific data also shed light on an alternative COOH-H-abstraction mechanism observed in specific cases, as simulations show that H abstraction in the case of IIn and VIIp glycine conformers is preceded by internal H transfer from the carboxyl group to the amino group, leading to the formation of a transient H_3N–CH_2–COO biradical intermediate. The structural arrangement of IIn and VIIp reactant conformers promotes H-migration by positioning the carboxyl-H close to the amino-N, creating favorable conditions for biradical formation. The animations further revealed that once H is abstracted from the carboxyl group, the resulting H_2NCH_2COO• intermediate can stabilize not only via fragmentation, but also through structural rearrangement as a minor pathway, involving an intramolecular H shift from the amino-N to the COO group, forming a species that corresponds to the product of the NH_2-H-abstraction reaction. An examination of conformer-specific product distributions indicates that structural changes in the carboxyl group follow a

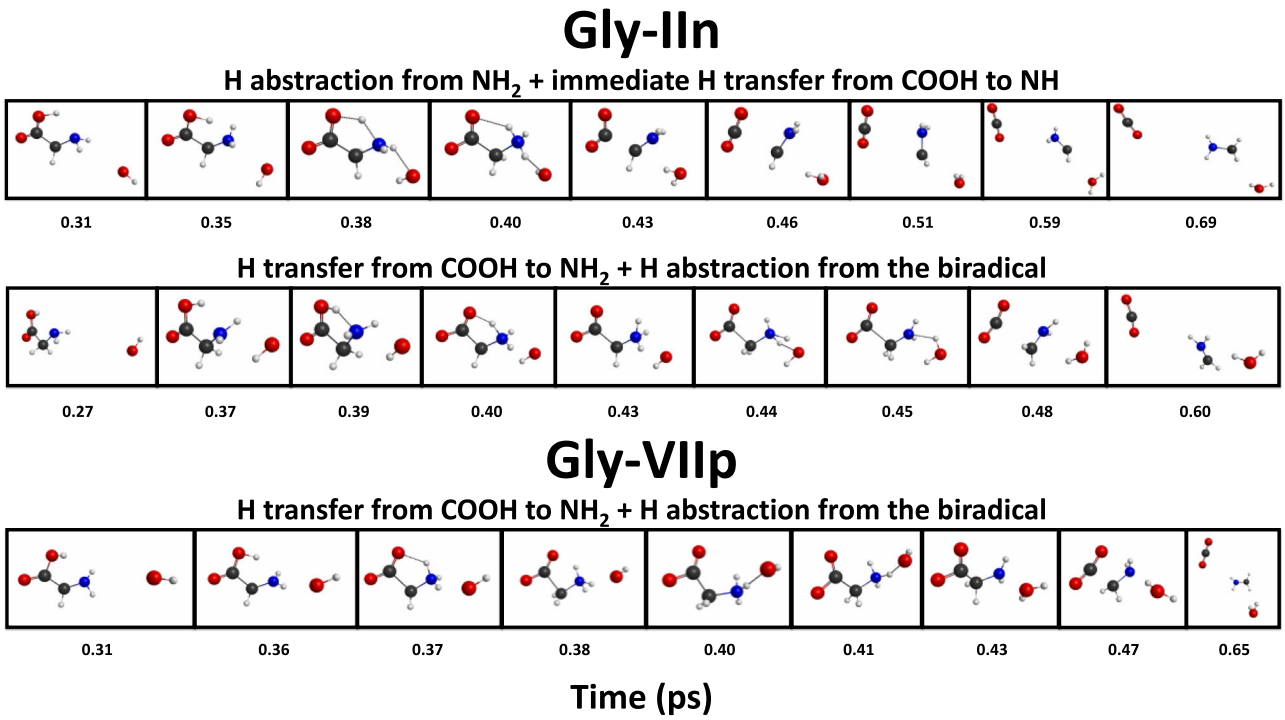

Fig. 5 | Intramolecular H-transfer pathways for the OH + glycine → $H_2O + CO_2 + CH_2NH_2$ reaction. Snapshots of representative trajectories for the H-abstraction reaction of the IIn and VIIp glycine conformers with OH attacking the amino site, occurring via intramolecular H transfer and resulting in H_2O, CO_2, and CH_2NH_2 products. Cartesian coordinates for each frame are given in Supplementary Data 3.

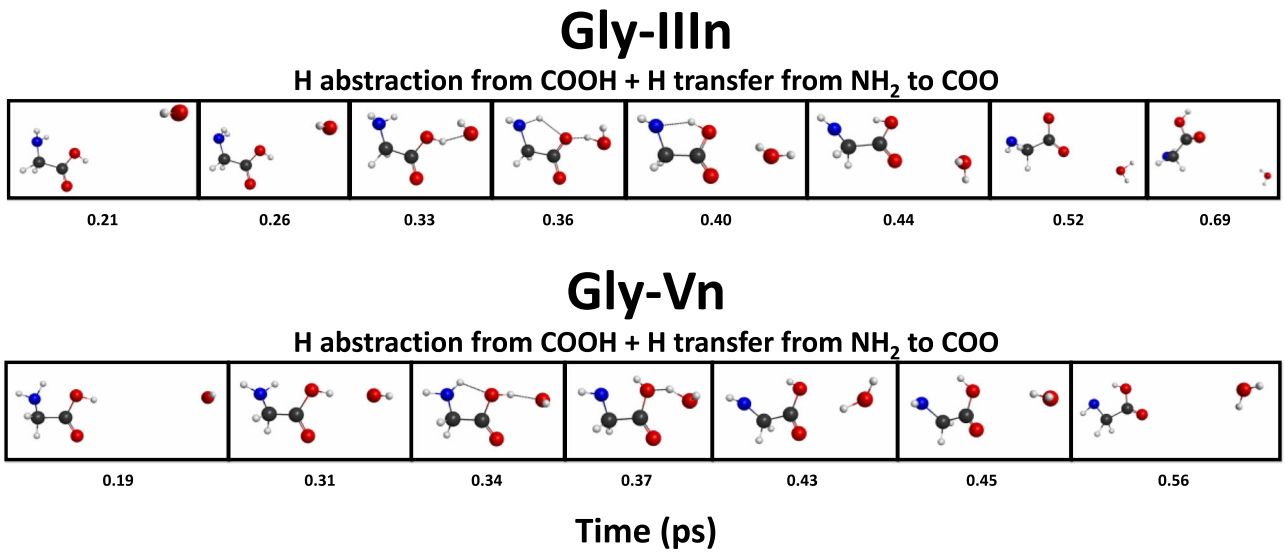

Fig. 6 | Intramolecular H-transfer pathways for the OH + glycine → $H_2O + HNCH_2COOH$ reaction. Snapshots of representative trajectories for the H-abstraction reaction of the IIIn and Vn glycine conformers with OH attacking the carboxyl site, occurring via intramolecular H transfer and resulting in $H_2O + HNCH_2COOH$ products. Cartesian coordinates for each frame are given in Supplementary Data 3.

probability-based sequence during H-abstraction reactions: an initial rearrangement of the carboxyl-H atom occurs most frequently, followed by a 180° rotation of the carboxyl group, while the simultaneous occurrence of both transformations is the least likely. The probability of large-scale structural changes, such as a complete 180° carboxyl rotation, remains low in CH_2-H-abstraction but is more frequent in NH_2-H-abstraction when hydrogen bonding is significantly altered. Furthermore, the closed conformation of the carboxyl group proves far more favorable than the open arrangement. Product distributions also show that CH_2-H-abstraction emerges as the only pathway capable of selectivity, where specific reactant conformers predominantly yield a single product conformer. Selectivity is linked to the initial conformation of the carboxyl group, which dictates whether structural rearrangements occur during the reaction. In contrast, NH_2-H-abstraction disrupts hydrogen bonding, increasing molecular flexibility and leading to a broader range of product conformers. Altogether, the presented findings not only deepen the mechanistic understanding of glycine oxidation but also provide a framework for exploring site- and conformer-specific dynamics of analogous complex processes in related biomolecular and atmospheric systems.

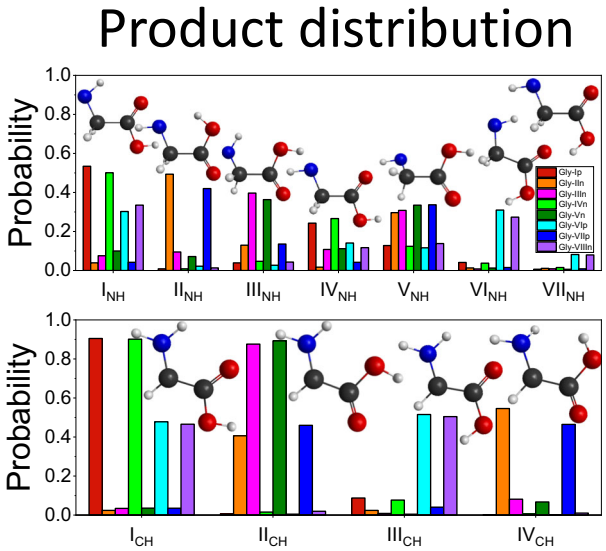

Fig. 7 | Conformer-specific product distributions of the OH + glycine system. Product distributions of the OH + glycine NH_2- and CH_2-H-abstraction reactions, where each histogram represents a different initial glycine conformer and the product conformer structures are displayed above the columns. The distributions are normalized over the various product conformers. Numerical values are given in Supplementary Data 2.

Methods

The computational study of the OH + glycine reaction involves the development of a full-dimensional PES and the application of QCT simulations to investigate reaction dynamics. The PES is constructed using high-level quantum chemical methods, including an explicitely-correlated version of the gold-standard coupled-cluster approach[37], to provide an accurate description of the motion of the electrons. The development of the PES is carried out automatically following the generation of an initial set of geometries, which are derived from the previously-identified[33,35] stationary points. This automated process, performed using the machine-learning-type ROBOSURFER program package[38], ensures comprehensive sampling of relevant configurations, facilitating an accurate representation[39] of the potential energy landscape. To unravel the reaction dynamics, the QCT method[40] is employed. By treating nuclear motion classically while ensuring that the vibrational energies of the reactants correspond to their ZPE, QCT bridges the gap between accuracy and computational feasibility. By executing hundreds of thousands of simulations initiated from different glycine conformers, key reaction quantities are determined, including conformer-specific reaction probabilities, from which ICSs are derived, initial attack angle distributions of the reactants, and the relative abundances of different product conformers formed from various glycine structures. Further details on the applied methodologies and computational procedures can be found in the Supplementary Methods. Initial and final coordinates and velocities of the trajectories are given in Supplementary Data 1.

Online content

Additional computational details, T_1-diagnostic values, fitting errors, relative energies of the glycine conformers, assessment of statistical uncertainties, pictorial representation of the initial structure generation, and comparison of ab initio and PES energies along a representative trajectory, as well as initial-conformer-specific-reaction probabilities, scattering angle distributions, and initial attack angle distributions for the OH + Gly(X) [X = Ip, IIn, IIIn, IVn, Vn, VIp, VIIp, VIIIn] reactions. Source data for the main figures including initial and final coordinates and velocities of the trajectories.

Data availability

The data that support the findings of this study are available in Supplementary Tables 1−4 and Supplementary Data 1−3 as well as from the corresponding author upon reasonable request.

Received: 11 July 2025; Accepted: 20 November 2025;
Published online: 14 December 2025

References

1. Lee, Y. T. Molecular beam studies of elementary chemical processes. *Science* **236**, 793–798 (1987).
2. Lin, J. J., Zhou, J., Shiu, W. & Liu, K. State-specific correlation of coincident product pairs in the F + CD_4 reaction. *Science* **300**, 966–969 (2003).
3. Mikosch, J. et al. Imaging nucleophilic substitution dynamics. *Science* **319**, 183–186 (2008).
4. Schatz, G. C. & Kuppermann, A. Quantum mechanical reactive scattering: an accurate three-dimensional calculation. *J. Chem. Phys.* **62**, 2502–2504 (1975).
5. Czakó, G. & Bowman, J. M. Dynamics of the reaction of methane with chlorine atom on an accurate potential energy surface. *Science* **334**, 343–346 (2011).
6. Welsch, R. & Manthe, U. Fast Shepard interpolation on graphics processing units: potential energy surfaces and dynamics for H + CH_4 → H_2 + CH_3. *J. Chem. Phys.* **138**, 164118 (2013).
7. Qi, J. et al. Communication: Mode specific quantum dynamics of the F + CHD_3 ⟶ HF + CD_3 reaction. *J. Chem. Phys.* **144**, 171101 (2016).
8. Fu, B., Shan, X., Zhang, D. H. & Clary, D. C. Recent advances in quantum scattering calculations on polyatomic bimolecular reactions. *Chem. Soc. Rev.* **46**, 7625–7649 (2017).
9. Szabó, I. & Czakó, G. Revealing a double-inversion mechanism for the F^- + CH_3Cl S_N2 reaction. *Nat. Commun.* **6**, 5972 (2015).
10. Ayasli, A. et al. A dynamic isotope effect in the nucleophilic substitution reaction between F^- and CD_3I. *Nat. Commun.* **16**, 2318 (2025).
11. Papp, D., Tajti, V., Győri, T. & Czakó, G. Theory finally agrees with experiment for the dynamics of the Cl + C_2H_6 reaction. *J. Phys. Chem. Lett.* **11**, 4762–4767 (2020).
12. Gruber, B., Tajti, V. & Czakó, G. Full-dimensional automated potential energy surface development and dynamics for the OH + C_2H_6 reaction. *J. Chem. Phys.* **157**, 074307 (2022).
13. Lu, D. & Li, J. Mode specificity of a multi-channel reaction prototype: F + CH_3OH ⟶ HF + CH_3O/CH_2OH. *Theor. Chem. Acc.* **139**, 157 (2020).
14. Meyer, J. et al. Atomistic dynamics of elimination and nucleophilic substitution disentangled for the F^- + CH_3CH_2Cl reaction. *Nat. Chem.* **13**, 977–981 (2021).
15. Nacsa, A. B., Tokaji, C. & Czakó, G. High-level analytical potential-energy-surface-based dynamics of the OH^- + CH_3CH_2Cl S_N2 and E2 reactions in full (24) dimensions. *Faraday Discuss* **251**, 604–621 (2024).
16. Yang, X. State-to-state dynamics of elementary bimolecular reactions. *Ann. Rev. Phys. Chem.* **58**, 433–459 (2007).
17. Pan, H., Zhao, B., Guo, H. & Liu, K. State-to-state dynamics in mode-selective polyatomic reactions. *J. Phys. Chem. Lett.* **14**, 10412–10419 (2023).
18. Császár, A. G. Conformers of gaseous glycine. *J. Am. Chem. Soc.* **114**, 9568–9575 (1992).
19. Balabin, R. M. Conformational equilibrium in glycine: focal-point analysis and ab initio limit. *Chem. Phys. Lett.* **479**, 195–200 (2009).
20. Shemesh, D. & Gerber, R. B. Different chemical dynamics for different conformers of biological molecules: photoionization of glycine. *J. Chem. Phys.* **122**, 241104 (2005).

21. Mardyukov, A., Quanz, H. & Schreiner, P. R. Conformer-specific hydrogen atom tunnelling in trifluoromethylhydroxycarbene. *Nat. Chem.* **9**, 71–76 (2017).
22. Kilaj, A. et al. Conformer-specific polar cycloaddition of dibromobutadiene with trapped propene ions. *Nat. Commun.* **12**, 6047 (2021).
23. Champenois, E. G. et al. Conformer-specific photochemistry imaged in real space and time. *Science* **374**, 178–182 (2021).
24. Bazsó, G., Magyarfalvi, G. & Tarczay, G. Tunneling lifetime of the *ttc*/VIp conformer of glycine in low-temperature matrices. *J. Phys. Chem. A* **116**, 10539–10547 (2012).
25. Barone, V., Biczysko, M., Bloino, J. & Puzzarini, C. Accurate structure, thermodynamic and spectroscopic parameters from CC and CC/DFT schemes: the challenge of the conformational equilibrium in glycine. *Phys. Chem. Chem. Phys.* **15**, 10094–10111 (2013).
26. Nacsa, A. B. & Czakó, G. Benchmark ab initio proton affinity of glycine. *Phys. Chem. Chem. Phys.* **23**, 9663–9671 (2021).
27. Yu, D., Rauk, A. & Armstrong, D. A. Radicals and ions of glycine: an ab initio study of the structures and gas-phase thermochemistry. *J. Am. Chem. Soc.* **117**, 1789–1796 (1995).
28. Galano, A., Alvarez-Idaboy, J. R., Montero, L. A. & Vivier-Bunge, A. OH hydrogen abstraction reactions from alanine and glycine: a quantum mechanical approach. *J. Comput. Chem.* **22**, 1138–1153 (2001).
29. Croft, A. K., Easton, C. J. & Radom, L. Design of radical-resistant amino acid residues: a combined theoretical and experimental investigation. *J. Am. Chem. Soc.* **125**, 4119–4124 (2003).
30. Huang, Y., Guler, L., Heidbrink, J. & Kenttämaa, H. Reactions of charged phenyl radicals with aliphatic amino acids in the gas phase. *J. Am. Chem. Soc.* **127**, 3973–3978 (2005).
31. Yang, G., Zu, Y. & Zhou, L. Deprotonation and radicalization of glycine neutral structures. *J. Phys. Org. Chem.* **21**, 34–40 (2008).
32. Carbonniere, P., Dargelos, A., Ciofini, I., Adamo, C. & Pouchan, C. Vibrational analysis of glycine radical: a comparative ab initio static and dynamic study. *Phys. Chem. Chem. Phys.* **11**, 4375–4384 (2009).
33. Orján, E. M., Nacsa, A. B. & Czakó, G. Conformers of dehydrogenated glycine isomers. *J. Comput. Chem.* **41**, 2001–2014 (2020).
34. Lin, R.-J., Wu, C.-C., Jang, S. & Li, F.-Y. Variation of reaction dynamics for OH hydrogen abstraction from glycine between ab initio levels of theory. *J. Mol. Model.* **16**, 175–182 (2010).
35. Gruber, B. & Czakó, G. High-level ab initio mapping of the multiple H-abstraction pathways of the OH + glycine reaction. *Phys. Chem. Chem. Phys.* **25**, 5271–5281 (2023).
36. Raghavachari, K., Trucks, G. W., Pople, J. A. & Head-Gordon, M. A fifth-order perturbation comparison of electron correlation theories. *Chem. Phys. Lett.* **157**, 479–483 (1989).
37. Knizia, G., Adler, T. B. & Werner, H.-J. Simplified CCSD(T)-F12 methods: theory and benchmarks. *J. Chem. Phys.* **130**, 054104 (2009).
38. Győri, T. & Czakó, G. Automating the development of high-dimensional reactive potential energy surfaces with the Robosurfer program system. *J. Chem. Theory Comput.* **16**, 51–66 (2020).
39. Xie, Z. & Bowman, J. M. Permutationally invariant polynomial basis for molecular energy surface fitting via monomial symmetrization. *J. Chem. Theory Comput.* **6**, 26–34 (2010).
40. Hase, W. L. *Encyclopedia of Computational Chemistry* 399–407 (Wiley, 1998).

Acknowledgements

We thank the National Research, Development and Innovation Office–NKFIH, K-146759; Project no. TKP2021-NVA-19, provided by the Ministry of Culture and Innovation of Hungary from the National Research, Development and Innovation Fund, financed under the TKP2021-NVA funding scheme; and the Momentum (Lendület) Program of the Hungarian Academy of Sciences for the financial support. We thank Dr. Viktor Tajti for his help with the PES development.

Author contributions

G.C. conceived the project; B.G. performed the computations and analyzed the data; and B.G. and G.C. wrote the paper.

Competing interests

The authors declare no competing interests.

Additional information

Supplementary information The online version contains supplementary material available at https://doi.org/10.1038/s42004-025-01823-5.

Correspondence and requests for materials should be addressed to Gábor Czakó.

Peer review information *Communications Chemistry* thanks Bina Fu and Tetsuya Taketsugu for their contribution to the peer review of this work. A peer review file is available.